Towards Surgical Subtask Automation—Blunt Dissection

Renáta Elek*, Tamás D. Nagy*, Dénes Á. Nagy*†, Tivadar Garamvölgyi*, Bence Takács*, Péter Galambos*, József K. Tar*, Imre J. Rudas* and Tamás Haidegger*†
*Antal Bejczy Center for Intelligent Robotics, Óbuda University, Budapest, Hungary
†Austrian Center for Medical Innovation and Technology (ACMIT), Wiener Neustadt, Austria
Email: {renata.elek, tamas.daniel.nagy, denes.nagy, tivadar.garamvolgyi, bence.takacs, peter.galambos, jozsef.tar, imre.rudas, tamas.haidegger}@irob.uni-obuda.hu

***Abstract*—Robot-assisted Minimally Invasive Surgical techniques are becoming standard-of-care in the surgical practice. With the rapid advancement of surgical robotics, many believe that the next step is subtask automation, since it has the potential to safely improve one element of a surgery, which might be most suitable for design and execution supported by artificial intelligence. The outcome of surgery may significantly improve from partial automation already, patient given better accuracy and targeting. This technology can also help surgeons efficiently with time-consuming operations. In this paper, we demonstrate the automation of *blunt dissection*, which is a common element in almost all abdominal procedures. Blunt dissection is regularly performed during Laparoscopic Cholecystectomy, e.g., when the surgeon exposes the Calot triangle. Automating this episode would streamline the procedure, and multiple similar automated sub tasks can be integrated into the surgical workflow. The presented method only relies on the images of a stereo camera system, and therefore does not put any additional overhead on the Operating Theater. The method was successfully tested in vitro and ex vivo in simplified simulated environment.**

I. Introduction

Technology is rapidly forming the field of surgery, and Minimally Invasive Surgical (MIS) techniques are becoming standard of care [1]. Furthermore surgical robotics can provide a platform to extend the human operator's dexterity and accuracy through teleoperation and navigation. Since robotic platforms—such as the da Vinci Surgical System (Intuitive Surgical Inc., Sunnyvale, CA)—have already been widely used for over 20 years, many believe that the next step in technology development is surgical automation [2], [3], [4], [5]. To achieve this goal it is important that the algorithms take into considerating the actual surgical workflow, where Surgical Process Models (SPM) provide detailed information on several granularity levels on how surgery is built up [6], [7], [8]. In this work, blunt dissection, a common element of subtask level SPMs is targeted for automation. The subtask level SPM granularity was chosen because the processes on this ontology level are non procedure specific surgical techniques, but they are detailed enough, to be accurately defined for automation. Later, these procedure elements can be applied onto different procedures, eventually creating a dictionary to build up more complex procedures for a wide variety of operations.

Blunt dissection is a surgical subtask, where the surgeon carefully separates two tissue layers without using the instruments cutting edges in an effort to avoid any damage to sensitive tissue structures (e.g., vessels, nerves). During blunt dissection, the retractor keep the tissues and the dissector is inserted between the two layers, then by opening of the dissector it forces the two layers apart. This surgical subtask is recurring element in multiple procedures, where automation could ease the cognitive load on the surgeon by relieving him/her from concentrating onto the manuality of the instruments,so the surgeon may pay full attention to the patient specific details of the surgery. Furthermore, robotically executed procedures can provide an increased accuracy compared to the human operator, therefore it can effect the success of the operation. In this work, we demonstrate a method for the automation of blunt dissection surgical subtask implemened through the example of Laparoscopic Cholecystectomy (LC).

II. Materials and Methods

A. Surgical phantom

During LC procedures, blunt dissection is a commonly employed subtask to open up the Calot triangle (Fig. 1). To validate our automated method, a surgical phantom was created. The phantom consists of two layers of solid silicone connected by a softer, dissectible layer. This soft layer simulates the connective tissue, which can be penetrated and dissected with a blunt surgical tool. Naturally, the human abdominal space consists of much more complex tissue structures, with varying properties. These will also be incorporated in our later experiments via sophisticated soft tissue parametrization [9].

B. Image Processing

When designing algorithms for the Operating Room (OR) environment, it is an important requirement that the new method should fit into the existing workflow, and should not introduce obstructive new equipment into the OR. With this principle in mind, we choose to base our algorithm on stereo video feed, as it is a common—and for the majority of cases the only—sensory input, such as the da Vinci.

In our test environment, two web cameras (Logitech C525—Logitech, Romanel-sur-Morges, Switzerland) were used to provide the stereo image feed. The cameras were placed in a stable frame within 50 mm distance from each other, and the custom created blunt dissection phantom was fixed on a

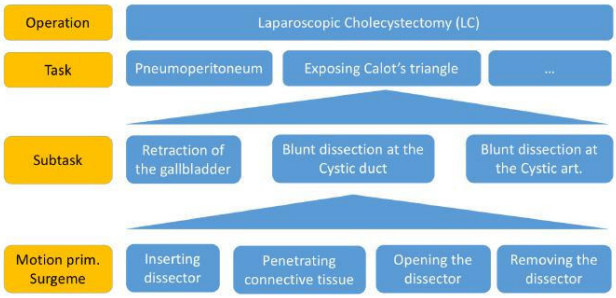

Fig. 1. Decomposition and mapping of the Laparoscopic Cholecystectomy procedure onto different granularity levels.

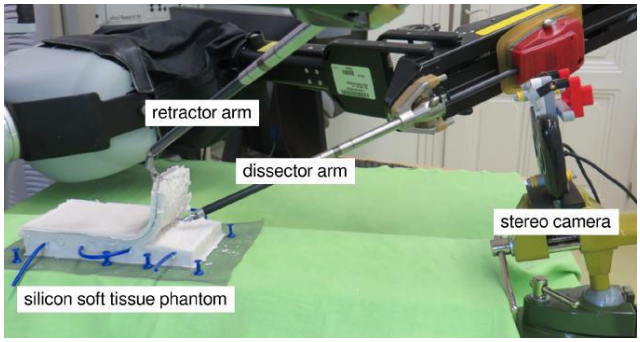

Fig. 2. Automated blunt dissection test setup at IROB. The DVRK (http://research.intusurg.com/dvrkwiki)-enabled da Vinci Surgical System, a dissection phantom and a camera were involved.

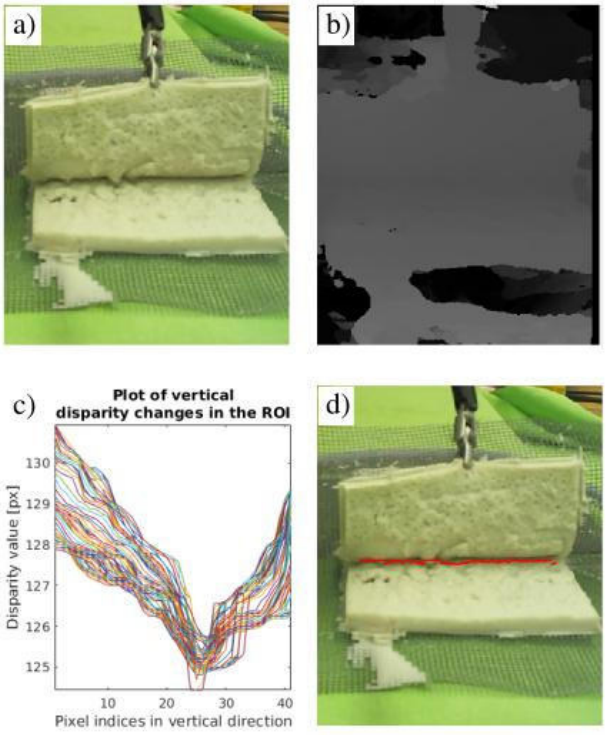

Fig. 3. Method for blunt dissection automation via computer vision. a) Image of blunt dissection phantom; b) disparity map of the field of view (greyscale represents the points' distances from the camera); c) plot of disparity changes in vertical direction; d) blunt dissection profile from the local minime of the disparity map.

stiff surface in approximately 350 mm from the viewpoint of the cameras. The cameras were used with 640x480 pixel resolution in MATLAB 2016b, and the focal length was fixed.

To estimate the depth in the field of view with a stereo system, it is crucial to calibrate the cameras. We performed the stereo camera calibration with 19 image pairs of a checkerboard pattern (with the checkerboard size being 25 x 25 mm). For every case, we fixed the pattern to a flat surface, as distortions in the pattern can greatly affect the calibration. To achieve better calibration accuracy, it is important for the the checkerboard pattern to be kept of an equal distance from the camera, within the expected field of interest. During the calibration, the pattern was placed at different orientations relative to the camera, and besides, the center points of the pattern were moved close to the frame edges as well to account for lens distortion. After the calibration the reprojection errors are calculated, which consist of the error between the reprojected point in the camera and the detected point. MATLAB Stereo Camera Calibrator App calculated reprojection errors by projecting the checkerboard points from world coordinates (determined by the checkerboard) into image coordinates. The Camera Calibrator App then compared the reprojected points to the corresponding detected points. Reprojection errors are acceptable if they are closer than one pixel [10].

The targeting system relies on the disparity map of the scene. Disparity map is the distance between two corresponding points (pixels) in the images of camera1 and camera2 stereo pair. Prior to the operation, the mentioned stereo camera calibration was performed for accurate image rectification and disparity map reconstruction during the procedure. For the depth calculation, a pixel-wise matching algorithm called Semi-Global Block Matching (SGBM) method (implemented in MATLAB 2016b) was used [11]. SGBM employs pixelwise matching based on Mutual Information and the approximation of a global smoothness constraint. SGBM was chosen because it is highly robust, and has a good computational time performance.

The process presented in Fig. 3 is initiated by manually selecting a starting and an end point of the blunt dissection line. Between these boundary points, the precise target points—where the dissection profile is optimal—are automatically selected. This is achieved by searching for the local minima (on a smoothed surface: moving average) in the depth dimension of the 3D surface (Fig. 3). If the dissection points have homogeneous local disparity environment, and the search algorithm cannot find peaks, the algorithm determines the disparity values from the initialized start and stop points. The accuracy is furtherly increased by removing the outliers using Hampel filter after the detection of the dissection line. To allow the dissection to progress evenly on the dissection line, the algorithm always chooses the smallest depth area on the detected dissection profile as the next target.

The success of this computer vision method is dependent on environment factors such as light, noises, etc. To avoid complications caused by these factors, built-in functions are necessary. It may be important to know the earlier positions of the target objection and the dissection line. For this reason, we developed a segmentation method to detect the Region Of Interest (ROI) on the image. This segmentation method is based on the depth of the start and end points of the dissection line; this way, if the surgeon chooses the right points, the ROI can be easily detectable. The state machine (see later) knows the last position of the dissection line, and it searches for the last local environment of the last line. We filter invalid disparity values as well to avoid inaccurate position coordinates.

C. Robot control

For the demonstration of the automated blunt dissection procedure, the da Vinci Surgical System was used, accessing the robot control trough the da Vinci Research Kit (dVRK) [12], [13], [14]. In this setup, the da Vinci provides a test environment similar to clinical setups available at many institutions. The da Vinci system is widely used in the everyday clinical practice worldwide (yearly, more than 500 000 procedure are performed only in the USA) and the dVRK provides a convenient programming platform by interfacing the Robot Operating System (ROS). We established the transformation between the robot's base frame and the 3D image coordinate system by performing a standard hand-eye calibration, using a small checkerboard pattern attached onto the tooltip [15]. This checkerboard can be robustly detected in the camera images, and then, can be used to determine the transformation matrix. Images were captured by both cameras simultaneously in different tool positions, and the coordinates of the tool were calculated from the detected checkerboard positions on the images. Cartesian positions are received from the DVRK in the robot coordinate system, after which the transformation between the two coordinate frames are determined by rigid frame registration. At the beginning of the blunt dissection procedure, we place the top tissue layer under a constant retraction force, which is achieved by using the 2nd arm of the da Vinci robot. The dissection process is built of simple motion primitives as shown in Fig. 5. The program starts by finding the target on the object. The dissector arm approaches the target, and the tool penetrates the tissue layers. Then, the grippers are opened, and the tool is pulled out, separating the two layers in the tools small local environment. After this, the grippers are closed again, and the tool is moved out of the scene, allowing a new stereo image to be captured. One iteration of the dissection process separates the tissue layers in a small local region, and the Computer Vision Node captures a new stereo image, and checks if the task is done by examining if the target is exposed; if the target structure is exposed, the agent stops, otherwise the loop resets on a new dissection target point (Fig. 4).

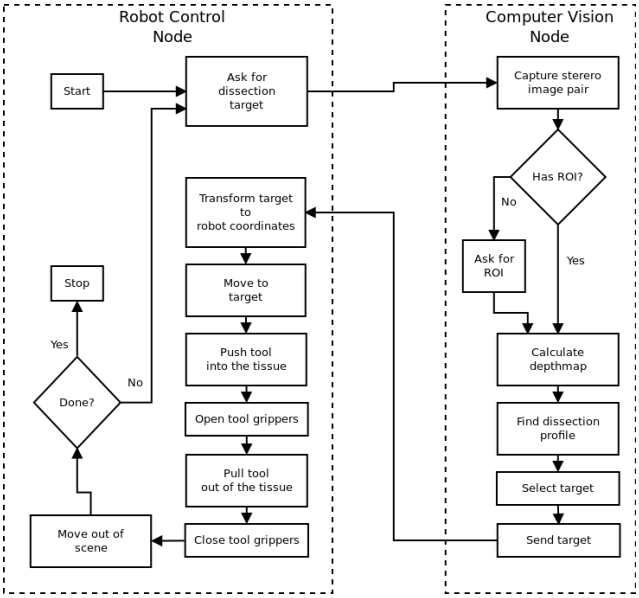

Fig. 4. Flow diagram of the automated blunt dissection method. The Computer Vision Node operates as the master, by selecting the the target points of the blunt dissection, and the Robot Control Node dissects the phantom on the targeted area.

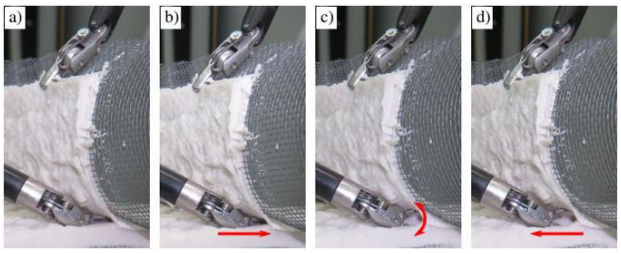

Fig. 5. Motion primitives of the surgical subtask automation. a) The surgical instrument (large needle driver) moves to the dissection target; b) the robot pushes the instrument into the phantom; c) instrument is opened; d) the robot pulls out the instrument, and moves to the next target.

III. Results

We validated our camera calibration accuracy with the mean pixel error from 10 calibration. The average of the mean pixel errors was 0.104 px, with standard deviation of 0.0165 px. In each of the 10 calibration sessions 19 image pairs were used of whom averagely 2.2 pairs were rejected (checkerboard detection or outlier).

The accuracy of the depth estimation of the system was tested on a planar white and a checkerboard pattern paper. The depth of these objects was measured on different distances from the camera pair (Fig. 6). The mean error and the average of the standard deviation was 4.1 and 0.7 mm respectively. The robot control accuracy was derived from 10 test cases, an average of 2.2 mm accuracy was achieved with a standard deviation of 0.5 mm in the camera views plane. In the depth axis the algorithm achieved 1 mm accuracy with standard deviation of 0.6 mm. The overall performance of the algorithm

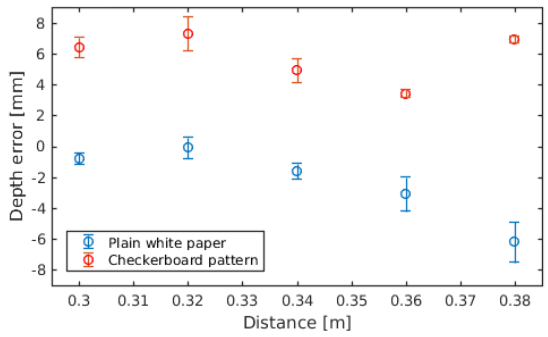

Fig. 6. Depth error of the objects with known surface on different distances from the stereo camera.

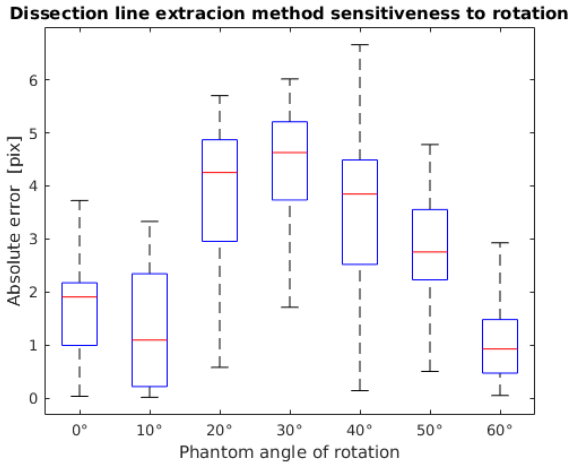

Fig. 7. Absolute error of the dissection line extraction method sensitiveness to rotation. Rotation was not significantly influence the algorithm.

was evaluated on the silicone-based custom designed phantom. Single dissections were made on 25 different locations on the dissection profile, of whom 21 succeeded; in 4 of the locations, the tool missed the dissection profile by a maximum of 3 mm.

We tested the dissection line detection methods sensitiveness to rotation. For this, we used the blunt dissection phantom. We rotated the phantom from 0 to 60 degrees relative to the camera. We found that our method is not significantly sensitive to rotation; our method worked acceptable in every cases as it is shown in Fig. 7.

We also tested our dissection line detection methods sensitivity to texture. For this, we used four types of paper (plain white, checkerboard pattern, rough surfaced and kraft paper) and the dissection phantom. We kept the phantom and the papers in opened state to simulate retraction. In all of the cases, the algorithm had to find a linear dissection profile. We chose the start and end point on the objects with 100 mm distance of each other; these points were the ground truth of the dissection line points. The objects placed from the stereo system approximately 500 mm distance. We found that our method is highly sensitive to the texture and the pattern of the objects. The method worked well on feature–rich objects (with the checkerboard pattern, kraft paper and the dissection phantom), but it failed on feature poor objects (plain white paper and rough surface paper). For the results see Fig. 8.

The computer vision method was tested in ex vivo envi-

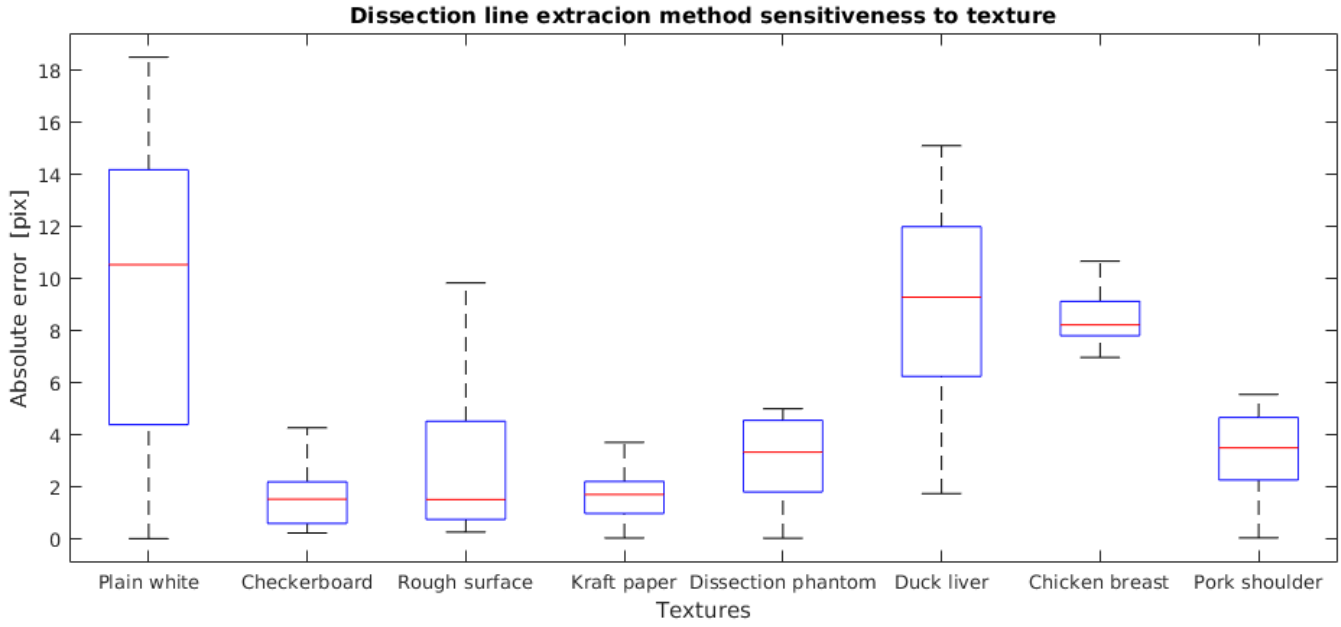

Fig. 8. Absolute error of the dissection line extraction method sensitivity to texture. The number of features and the shining of the objects are crucial in the detection of the dissection line.

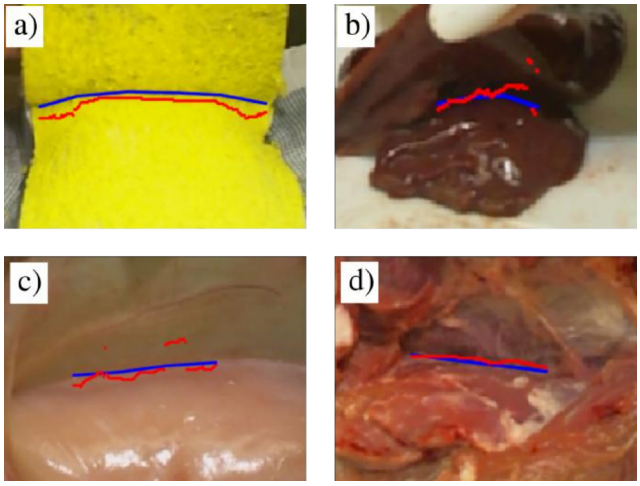

Fig. 9. Dissection line detection tests in vitro and ex vivo environment. a) Blunt dissection surgical phantom; b) duck liver; c) chicken breast; d) pork shoulder. The method is very sensitive to shining (see liver), and feature-richness (see chicken breast).

ronment as well. We used a chicken breast, a pork shoulder and a duck liver to test the accuracy of the detection of the dissection line. We performed the sensitivity test on the ex vivo objects: we selected 6 points as the basis of comparison between the ground truth points and the detected points. We found that the method is sensitive to the texture of the object and to the lighting conditions. The method worked well on the pork shoulder, and it worked acceptable on the chicken breast and the duck liver. The reason is that pork is feature-rich, but the liver and the chicken breast are feature-poor and creates reflections (Fig. 9).

IV. Conclusion and Discussion

In this paper, we presented a surgical subtask automation method. The demonstrated algorithm for blunt dissection is based on depth perception, which was developed and tested as a proof of concept, and provided satisfactory initial results in a simplified phantom environment, as well as in ex vivo experiments. The method relies only on the video feed of a stereo-system, which is available in most da Vinci type surgical robots, and thus the method is easily integrable into clinical applications.

Further development is needed to examine better implementations for ex vivo experiments, where inhomogeneity of the tissue, the environment and the tool–tissue interaction are better accounted. Trials are necessary to confirm the reliability of the method under real surgical conditions. Further improvements could be implemented on the robot's motion by implementing learning-by-observation approaches, these methods are yet to be tested.

Acknowledgment

The research was supported by the Hungarian OTKA PD 116121 grant. This work has been supported by ACMIT (Austrian Center for Medical Innovation and Technology), which is funded within the scope of the COMET (Competence Centers for Excellent Technologies) program of the Austrian Government. T. Haidegger is supported through the New National Excellence Program of the Ministry of Human Capacities. Partial support of this work comes from the Hungarian State and the European Union under the EFOP-3.6.1-16-2016-00010 project.

References

[1] Á. Takács, D. Á. Nagy, I. Rudas, and T. Haidegger, "Origins of surgical robotics: From space to the operating room," vol. 13, no. 1, pp. 13–30.

[2] S. Sen, A. Garg, D. V. Gealy, S. McKinley, Y. Jen, and K. Goldberg, "Automating multi-throw multilateral surgical suturing with a mechanical needle guide and sequential convex optimization," in *2016 IEEE International Conference on Robotics and Automation (ICRA)*, 2016, pp. 4178–4185.

[3] A. Murali, S. Sen, B. Kehoe, A. Garg, S. McFarland, S. Patil, W. D. Boyd, S. Lim, P. Abbeel, and K. Goldberg, "Learning by observation for surgical subtasks: Multilateral cutting of 3D viscoelastic and 2D Orthotropic Tissue Phantoms," in *2015 IEEE International Conference on Robotics and Automation (ICRA)*, 2015, pp. 1202–1209.

[4] H. C. Lin, I. Shafran, D. Yuh, and G. D. Hager, "Towards automatic skill evaluation: Detection and segmentation of robot-assisted surgical motions," *Computer Aided Surgery*, vol. 11, no. 5, pp. 220–230, 2006.

[5] T. Osa, K. Harada, N. Sugita, and M. Mitsuishi, "Trajectory planning under different initial conditions for surgical task automation by learning from demonstration," in *2014 IEEE International Conference on Robotics and Automation (ICRA)*, 2014, pp. 6507–6513.

[6] T. Neumuth, S. Schumann, G. Strauß, and P. Jannin, "Visualization Options for Surgical Workflows," *In. J. Comput Assist. Radiol. Surg.*, pp. 438–440, 2006.

[7] C. MacKenzie, Ibbotson AJ, Cao CGL, and Lomax A, "Hierarchical decomposition of laparoscopic surgery: A human factors approach to investigating the operating room environment." *Minim Invasive Ther Allied Technol*, vol. 10, no. 3, pp. 121–128, 2001.

[8] C. E. Reiley and G. D. Hager, "Task versus Subtask Surgical Skill Evaluation of Robotic Minimally Invasive Surgery," in *LNCS 5761*, vol. Part I. Springer-Verlag Berlin Heidelberg, 2009, pp. 435–442.

[9] Á. Takács, L. Kovács, I. Rudas, R.-E. Precup, and T. Haidegger, "Models for force control in telesurgical robot systems," vol. 12, no. 8, pp. 95–114.

[10] "Stereo Calibration App - MATLAB & Simulink," https://www.mathworks.com/help/vision/ug/stereo-camera-calibrator-app.html.

[11] H. Hirschmuller, "Accurate and efficient stereo processing by semi-global matching and mutual information," in *2005 IEEE Computer Society Conference on Computer Vision and Pattern Recognition (CVPR'05)*, vol. 2, 2005, pp. 807–814.

[12] G. S. Guthart and J. K. J. Salisbury, "The IntuitiveTM Telesurgery System: Overview and Application," in *2000 IEEE International Conference on Robotics and Automation*, San Francisco, CA, 2000, pp. 618–621.

[13] P. Kazanzides, Zihan Chen, Anton Deguet, Gregory S. Fischer, Russell H. Taylor, and Simon P. DiMaio, "An open-source research kit for the da Vinci® Surgical System," in *2014 IEEE International Conference on Robotics and Automation (ICRA)*, 2014.

[14] Á. Takács, I. Rudas, and T. Haidegger, "Open-Source Research Platforms and System Integration in Modern Surgical Robotics," *Acta Universitatis Sapientiae Electrical and Mechanical Engineering*, vol. 14, no. 6, pp. 20–34, 2015.

[15] J. B. A. Maintz and M. A. Viergever, "A survey of medical image registration," *Medical Image Analysis*, vol. 2, no. 1, pp. 1–36, 1998.